Radial Meixner Moment Invariants for 2D and 3D Image Recognition[1]

M. El Mallahi*, A. Zouhri, and H. Qjidaa

Sidi Mohamed Ben Abdellah University, Faculty of Sciences Dhar el Mahraz, Fez, Morocco

**e-mail: mostafa.elmallahi@usmba.ac.ma*

Abstract—In this paper, we propose a new set of 2D and 3D rotation invariants based on orthogonal radial Meixner moments. We also present a theoretical mathematics to derive them. Hence, this paper introduces in the first case a new 2D radial Meixner moments based on polar representation of an object by a one-dimensional orthogonal discrete Meixner polynomials and a circular function. In the second case, we present a new 3D radial Meixner moments using a spherical representation of volumetric image by a one-dimensional orthogonal discrete Meixner polynomials and a spherical function. Further 2D and 3D rotational invariants are derived from the proposed 2D and 3D radial Meixner moments respectively. In order to prove the proposed approach, three issues are resolved mainly image reconstruction, rotational invariance and pattern recognition. The result of experiments prove that the Meixner moments have done better than the Krawtchouk moments with and without nose. Simultaneously, the reconstructed volumetric image converges quickly to the original image using 2D and 3D radial Meixner moments and the test images are clearly recognized from a set of images that are available in a PSB database.

Keywords: 2D and 3D radial Meixner moments, volumetric image, 2D and 3D rotation invariants

DOI: 10.1134/S1054661818020128

1. INTRODUCTION

The 3D object recognition and 3D pattern classification play crucial roles and interesting part of image analysis tasks and computer vision. In general, 3D image classification or recognition is obtained by looking for descriptors representing the 3D object without taking into account certain deformations and/or transformations.

3D moment invariants were demonstrated to be very great means for pattern representation and it has often been proved that 3D moment invariants act out efficiently in 3D object recognition [1].

Up to now, different kinds of 3D moment invariants to spherical transformations of the 3D object have been suggested. Among all transformations TRS (translation, scaling, and rotation) that have been analyzed in this context, rotation plays a crucial role.

3D image rotation is found almost in all our applications, though the imaging system is well established and the experiment has been developed in a laboratory. On the other hand, rotation is unimportant to deal with mathematically, for these causes, researches have been interested on invariants to rotation since the beginning.

With the quick improvement of mathematics and sensor, 3D image processing, arises engineering and practice thanks to its more precise and flexible descriptions of 3D images.

Without doubt, developing rotation invariants for 3D images has become an interesting topic in the computer vision community.

The moments are the coefficients of projections of the image on a polynomial basis. These latter are widely used in image analysis. Indeed, the theory of moments are considered as efficient descriptors of the images and have been used to extract the characteristics of the images for object recognition [2–13], edge detection [14], watermarking [15], and the compression [16]. Hu is the first to introduce the invariant geometric moments and defined seven descriptors for the classification of images. The geometrical moments are not orthogonal this causes the redundancy of the information when the use of these in the analysis of the images. To overcome this problem, Teague introduced the continuous orthogonal moments based on the polynomials of Legendre and Zernike. Recently, a series of discrete orthogonal moments such as Tchebichef moments, Krawtchouk moments, Meixner moments, Charlier moments and Hahn moments are used for the image representation [8, 9]. The use of discrete orthogonal moments based on discrete orthogonal polynomials eliminates the need for a numerical approximation and precisely satisfies the orthogonality property.

[1] The article is published in the original.

Received November 10, 2017

Comparing two images, Kazhdan [17] employed a similar phase correlation based on spherical harmonics.

In this specific example, it was employed for registration, but it can also be employed for recognition.

Fehr [18] describing an image composed of patches by employing the power spectrum and bispectrum calculated from a tensor function.

In [19], the same researcher used local binary object features and in [20] he employed harmonic local histograms of oriented gradients.

Compared to traditional geometric or complex moments, the most important advantage of orthogonal moments is their outstanding numerical stability, limited types of values, and the recurrent existing relations for their computation.

Therefore, many authors have tried to extract the 2D invariants from discrete orthogonal moments.

Yet, the extraction of 3D moments becomes more difficult than in 2D. The favorable numerical properties are still preserve by 3D orthogonal moments.

There are polynomials orthogonal inside a cube and others that are orthogonal on the sphere.

In the same way, the polynomials defined on a cube are less convenient than the sphere for extracting rotation invariants. This method was employed by Canterakis [21] using 3D continuous orthogonal Zernike moments.

In this paper, we suggest a new set of 2D and 3D rotation invariants based on discrete orthogonal radial Meixner moments as well as a theoretical mathematics to derive them. This paper introduces, in a first case, a new 2D radial Meixner moments employing polar representation of an object by a one-dimensional discrete Meixner polynomials and a polar function. In the second case, we present a new 3D radial Meixner moments employing a spherical representation of volumetric image by a one-dimensional discrete Meixner polynomials as well as a spherical function. Moreover, 2D and 3D rotational invariants are extracted from the suggested 2D and 3D radial Meixner moments respectively. We show that the transformation of Meixner moments under rotation may be inferred in an indirect way without clear investigation of this transformation.

Therefore, it is clear in the article that the rotation invariants from Meixner moments and from Krawtchouk moments have the same forms in 2D and 3D space.

This is an outstanding outcome because it permits to cat down rotation invariant extraction from Meixner moments to that from Krawtchouk moments in 2D and 3D space, which are not difficult to improve, still taking advantage from the image reconstruction of Meixner moments.

The transition from 2D to 3D is difficult and need a careful study because the 3D rotation has three degrees of freedom opposed to 2D rotation that has only one parameter.

Therefore, any 3D images and structures linked to rotation are richer than in 2D. What distinguishes between the 3D problem and the 2D is that rotation in 3D is not commutative.

That's why the generalization from 2D to 3D should be investigated carefully and not done automatically.

Such studies may find out a similarity with 2D and may come up with different outcomes.

The core idea of the proposed work is that the radial Meixner polynomials are orthogonal in ball and are more appropriate for extracting 2D and 3D rotation invariants. To prove the suggested method, three issues are resolved mainly 2D/3D image reconstruction, 2D/3D rotational invariance and pattern recognition. The result of the experiment prove that the Meixner moments have done better than the Krawtchouk moments in terms of 2D/3D image reconstruction capability. At the same time, the reconstructed 2D/3D image converges quickly to the original image using radial Meixner moments and the test of volumetric images are clearly recognized from a set of images that are found in a PSB database.

The rest of the paper is organized as follows. Section 2 presents an overflow to rotation invariant of 2D/3D Meixner moments. Section 3 introduces the simulation results of 2D/3D invariant Meixner moments. Finally, Section 4 concludes this paper.

2. THE ROTATION INVARIANT OF 2D/3D MEIXNER MOMENTS

In this section, we present a brief background of radial Meixner moments for 2D and 3D case.

2.1. 2D Radial Meixner Moments

In this subsection, we present a brief background of 2D radial Meixner moments based on the polar representation of a 2D image.

The rotational invariants are extracted from the radial Meixner moments. Radial polar coordinate of image intensity $f(r, \theta)$ are used to extract the radial moments by one-dimensional polynomials by a circular function. Figure 1 displays the region for computing the radial Meixner moments for an image of size $N \times N$ with ν and η represent the number of pixels along the radius r and perimeter, respectively.

The discrete angle θ_s is given by

$$\theta_s = \frac{2\pi s}{\eta} \tag{17}$$

with $s = 0, \ldots \eta - 1$.

The radial Meixner moments are presented as

$$M_{nm} = \frac{1}{\eta}\sum_{r=0}^{v-1}\sum_{s=0}^{\eta-1}\tilde{\omega}_n^{(\beta,\mu)}(x)e^{-i\frac{2\pi sm}{\eta}} f(r,\theta_s). \quad (1)$$

The transform inverse of moments are defined as

$$f(r,\theta_s) = \frac{1}{\eta}\sum_{n=0}^{\max-1}\sum_{m=0}^{\max-1}\tilde{\omega}_n^{(\beta,\mu)}(x)e^{i\frac{2\pi sm}{\eta}} M_{nm}. \quad (2)$$

The Cartesian coordinates (x, y) of each pixel will be obtained from the polar coordinate relations given by

$$\begin{cases} x = \dfrac{rN}{2(v-1)}\cos\left(\dfrac{2\pi s}{\eta}\right) + \dfrac{N}{2} \\ y = \dfrac{rN}{2(v-1)}\sin\left(\dfrac{2\pi s}{\eta}\right) + \dfrac{N}{2} \end{cases} \quad (3)$$

with $r = 0, 1, ..., v-1$ and $s = 0, 1, ..., \eta-1$.

To extract the rotational invariants of the radial Meixner moments we will use an image rotated by an angle θ' around the center of the ring.

The radial Meixner moments M'_{nm} with order $(n + m)$ for a rotated image is defined as

$$\begin{aligned} M'_{nm} &= \frac{1}{\eta}\sum_{r=0}^{v-1}\sum_{s=0}^{\eta-1}\tilde{\omega}_n^{(\beta,\mu)}(r)e^{-i\frac{2\pi(s-\theta')m}{\eta}} f(r,\theta_s) \\ &= e^{i\frac{2\pi\theta' m}{\eta}} M_{nm}. \end{aligned} \quad (4)$$

The norm of radial Meixner moment M' after the rotation is the same as the norm radial moment M

$$\begin{aligned} \left|M'_{nm}\right| &= \left|\frac{1}{\eta}\sum_{r=0}^{v-1}\sum_{s=0}^{\eta-1}\tilde{\omega}_n^{(\beta,\mu)}(r)e^{-i\frac{2\pi(s-\theta)m}{\eta}} f(r,\theta_s)\right| \\ &\times \left|e^{i\frac{2\pi\theta' m}{\eta}}\right| |M_{nm}| = |M_{nm}|. \end{aligned} \quad (5)$$

The $\phi_{nm} = |M_{nm}|$ are considered as the rotational invariants of the proposed radial Meixner moments.

2.2. 3D Radial Meixner Moments

To enlarge this method directly to 3D, we will use the Euler angles for any orientations/rotations in special orthogonal system in 3D case SO(3). With three successive rotations of angles $\theta \in [0, 2\pi]$, $\varphi \in [0, \pi]$, and $\psi \in [0, 2\pi]$ around the x, y, and z axes we can represent any three-dimensional rotation by

$$R = R_x(\theta)R_y(\varphi)R_z(\psi), \quad (6)$$

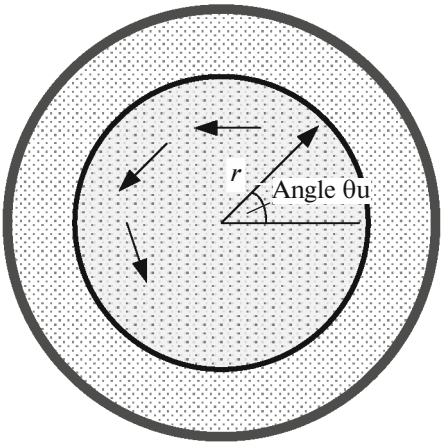

Fig. 1. The computation's region of radial Meixner moments.

where $R_x(\theta)$, $R_y(\varphi)$, and $R_z(\psi)$ are given by

$$\begin{aligned} R_x(\theta) &= \begin{pmatrix} 1 & 0 & 0 \\ 0 & \cos(\theta) & \sin(\theta) \\ 0 & -\sin(\theta) & \cos(\theta) \end{pmatrix}, \\ R_y(\theta) &= \begin{pmatrix} \cos(\varphi) & 0 & \sin(\varphi) \\ 0 & 1 & 0 \\ -\sin(\varphi) & 0 & \cos(\varphi) \end{pmatrix}, \\ R_z(\theta) &= \begin{pmatrix} 0 & 0 & 0 \\ \cos(\psi) & \sin(\psi) & 0 \\ -\sin(\psi) & \cos(\psi) & 1 \end{pmatrix}. \end{aligned} \quad (7)$$

The rotation of the volumetric images are only defined for any choice of angles with $\varphi \neq 0$. For $\varphi = 0$, we obtain a rotation of angle $\theta + \psi$ around the principal z-axis which are obtained by any mixture of values θ and ψ. This discretization is avoided by switching the values of φ by half of the step size of our discretization.

The 3D radial Meixner moments M_{klmn} with order $(k + n + m + l)$ for an image with intensity $f(r, \theta_s, \varphi_t, \psi_u)$ are defined as

$$\begin{aligned} M_{knml} &= \frac{1}{\eta+\delta+\lambda}\sum_{r=0}^{v-1}\sum_{s=0}^{\eta-1}\sum_{t=0}^{\delta-1}\sum_{u=0}^{\lambda-1}\tilde{\omega}_k^{(\beta,\mu)}(r) \\ &\times e^{-i\frac{2\pi sn}{\eta}} e^{-i\frac{2\pi tm}{\delta}} e^{-i\frac{2\pi ul}{\lambda}} f(r,\theta_s,\varphi_t,\psi_u), \end{aligned} \quad (8)$$

where

$$\begin{aligned} \theta_s &= \frac{2\pi s}{\eta}, \quad s = 0, 1, \ldots, \eta-1, \\ \varphi_t &= \frac{\pi t + 0.5}{\delta}, \quad t = 0, 1, \ldots, \delta-1, \\ \psi_u &= \frac{2\pi u}{\lambda}, \quad u = 0, 1, \ldots, \lambda-1. \end{aligned} \quad (9)$$

If the image is rotated randomly in steps of the given discretization defined by α', β', γ' the rotated 3D images will have in this case as intensity $f(r, \theta_{s+\alpha'}, \varphi_{t+\beta'}, \psi_{u+\gamma})$.

The moment of 3D radial Meixner moments noted M'_{knml} for the rotated image are given by

$$\begin{aligned} M'_{knml} &= \frac{1}{\eta+\delta+\lambda}\sum_{r=0}^{v-1}\sum_{s=0}^{\eta-1}\sum_{t=0}^{\delta-1}\sum_{u=0}^{\lambda-1}\tilde{\omega}_k^{(\beta,\mu)}(r) \\ &\times e^{-i\frac{2\pi sn}{\eta}} e^{-i\frac{2\pi tm}{\delta}} e^{-i\frac{2\pi ul}{\lambda}} f(r,\theta_{s+\alpha'},\varphi_{t+\beta'},\psi_{u+\gamma}) \\ &= \frac{1}{\eta+\delta+\lambda}\sum_{r=0}^{v-1}\sum_{s=0}^{\eta-1}\sum_{t=0}^{\delta-1}\sum_{u=0}^{\lambda-1}\tilde{\omega}_k^{(\beta,\mu)}(r) \\ &\times e^{-i\frac{2\pi(s-\alpha')n}{\eta}} e^{-i\frac{2\pi(t-\beta')m}{\delta}} e^{-i\frac{2\pi(u-\gamma')l}{\lambda}} f(r,\theta_s,\varphi_t,\psi_u) \\ &= e^{i\frac{2\pi\alpha' n}{\eta}} e^{i\frac{2\pi\beta' m}{\delta}} e^{i\frac{2\pi\gamma' l}{\lambda}} M_{knml}. \end{aligned} \tag{10}$$

The norm of 3D radial Meixner moment M' after the rotation is the same as the norm 3D radial moment M

$$|M'_{knml}| = |M_{knml}|.$$

The 3D radial Meixner rotational invariant called ϕ_{klmn} are defined by

$$\phi_{knml} = |M'_{knml}|. \tag{11}$$

2.3. The 2D and 3D Pattern Recognition

In this section, we present two new set of 2D and 3D radial Meixner moments invariants.

2.3.1. Characteristic vectors for 2D case. These 2D radial Meixner moments can then be used to form the descriptor vector of every 2D object. Specifically, the descriptor vector is composed of 2D radial Meixner moments up to order s, where s is experimentally selected.

The characteristic vectors V_{2D} is represented as

$$V_{2D} = [\phi_{nm} | n+m \in [0,1,\ldots s]]. \tag{12}$$

2.3.2. Characteristic vectors for 3D case. These 3D radial Meixner moments can then be also used to form the descriptor vector of every 3D object. Specifically, the descriptor vector is composed of 3D radial Meixner moments up to order s, where s is experimentally selected.

The characteristic vectors V_{3D} is represented as

$$V_{3D} = [\phi_{knml} | k+n+m+l \in [0,1,\ldots s]]. \tag{13}$$

2.3.3. 2D and 3D objet recognition. To perform the recognition of 2D and 3D objects to their appropriate classes. we use two method based on Euclidean distances and distance of correlations measuring the distance from V_{query} and V_{test} where V represent the characteristic vectors V_{2D} for 2D and V_{3D} for 3D case

$$d_{\text{Euclidean}}(V_{\text{query}}, V_{\text{test}}^K) = \sqrt{\sum_{j=0}^{T}(V_{\text{query}}^j - V_{\text{test}}^j)^2} \tag{14}$$

and

$$\begin{aligned} d_{\text{correlation}}(V_{\text{query}}, V_{\text{test}}^K) &= \sum_{j=0}^{T} V_{\text{query}}^j V_{\text{test}}^j \\ &\times \left|\sum_{j=0}^{r} V_{\text{query}}^j V_{\text{test}}^j\right|^{-\frac{1}{2}} \left|\sum_{j=0}^{r} V_{\text{query}}^j V_{\text{test}}^j\right|^{-\frac{1}{2}}, \end{aligned} \tag{15}$$

where the T-dimensional feature V_{query} is represented as

$$V_{\text{query}} = [V_{\text{query}}^1, V_{\text{query}}^2, \ldots V_{\text{query}}^T], \tag{16}$$

and the T-dimensional training vector of class K is represented as

$$V_{\text{test}}^K = [V_{\text{test}}^1, V_{\text{test}}^2, \ldots V_{\text{test}}^T]. \tag{17}$$

2.3.4. Classification criteria. Therefore, to classify the images, one takes the minimum values for $d_{\text{Euclidean}}$ and the maximum values for $d_{\text{correlation}}$.

The recognition precision is represented as

$$\xi = \frac{\text{Number of correctly classified volumetric images}}{\text{The number of volumetric images used in the test}} \times 100\%. \tag{18}$$

To prove the accuracy of the reconstruction, classification and recognition images using radial Meixner moment invariants for 2D and 3D image recognition, we will use two databases of image. Columbia Object Image Library database [23] in 2D case, and PSB database [24] in 3D case.

3. SIMULATION RESULTS

In this section, we present the simulation results of 2D and 3D radial Meixner moments invariant for the invariability, recognition and classification.

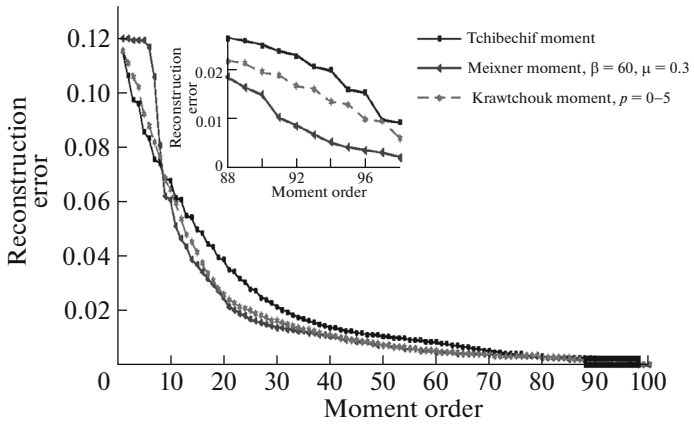

Fig. 2. Comparative study of reconstruction error of 3D Tchibechif, Krawtchouk, and Meixner moment.

3.1. Invariability for Radial Meixner Moment

In this subsection, we will discuss the invariability for 2D and 3D case.

3.1.1. Invariability for 2D radial Meixner moment. To validate the rotational invariant property of the radial Meixner moments, the same image Lena is selected Fig. 3. The image is rotated by 0°, 50°, 130°, and 230°. The selected order of the invariants Φ_{00}, Φ_{01}, Φ_{10}, Φ_{11} with $\eta = N/2$ and $\delta = 4N$ are computed for each of these images. The results are entered in Table 1.

To measure the similarity (changeability) of the proposed invariants under different image rotation, we will use the formula $\sigma/\mu(\%)$ where σ represent the standard deviation of radial Meixner's invariant moments for the different angle of each rotation, and μ is the average value.

The Table 1 show that the ratio σ/μ is very low and consequently the radial Meixner's moment invariants are very stable under different types of image rotation. Hence, the property of invariability of radial Meixner moments will be used to pattern recognition.

3.1.2. Invariability for 3D radial Meixner moment. To validate the rotational invariant property of the 3D radial Meixner moments, the 128 × 128 × 128 teddy bear image and there rotated version ($\phi = 10°$; $\theta = -90°$; $\psi = 120°$), ($\phi = 45°$; $\theta = 30°$; $\psi = -75°$), and ($\phi = -60°$; $\theta = -35°$; $\psi = -120°$) shown in Fig. 4 will be used. The selected order of the invariants Φ_{0000}, Φ_{0001}, Φ_{0010}, Φ_{0100}, Φ_{1000}, Φ_{0011}, Φ_{0101}, Φ_{1001}, and Φ_{1100} with $\eta = N/2$, $\delta = 4N$, $\mu = 4N$, and $\lambda = 4N$ are computed for each image.

The results of simulation are shown in Tables 2 taking $a = 10$, $b = 10$ for Meixner moment parameters.

Lastly, the ratio σ/μ can used to measure the capability of the proposed 3D rotation invariants under different image transformation.

Where σ represents the standard deviation of radial Meixner moment for the different factors of each rotation, and μ is the equivalent mean value.

The Table 2 show that the ratio σ/μ is very low and consequently the 3D radial Hahn' s moment invariants are very stable under different types of 3D image rotation. Hence, the property of invariability of radial Hahn moments well be used to pattern recognition.

Fig. 3. An image with various rotations.

Table 1. Selected order of rotational invariants of radial Meixner moments computed for Lena image with arbitrary rotation angles

θ', deg	Φ_{00}	Φ_{01}	Φ_{10}	Φ_{11}
θ' = 0	0.107335	0.074840	0.112730	0.063419
θ' = 30	0.103365	0.274847	0.102737	0.063414
θ' = 120	0.103365	0.274849	0.102739	0.063415
θ' = 230	0.103365	0.274850	0.102742	0.063418
σ/μ(%)	0.00 e00	1.492 e−03	8.272 e−04	6.870 e−03

3.2. Classification

In this subsection, we will discuss the classification for 2D and 3D case.

3.2.1. Classification for 2D radial Meixner moment. To validate the proposed approach for classification, we have taken the image from the Columbia object Library (COIL-20) database [22]. The total number of images is 1.440 distributed as 72 images for each object. All images of this database have the size 128 × 128. Figure 5 displays a collection of the six objects. The test set also is degraded by salt and pepper noise with noise densities 1, 2, 3, and 4%. The feature vector based on rotational Meixner's moment invariants is used to classify these images and its recognition accuracy is compared with that of radial Krawtchouk moment invariants. The results of the classification using all features are presented in Tables 3, 4.

3.2.2. Classification for 3D radial Meixner moment. To prove the proposed method for classification, we have taken the image from the Princeton Shape Benchmark (PSB) Database [24]. Being known, this database consists of 907 3D models classified into 35 main categories and 92 subcategories. All images of this database have the size 128 × 128 × 128. In Table 5, we find that the measure between the query of volumetric image and same images of classes from PSB

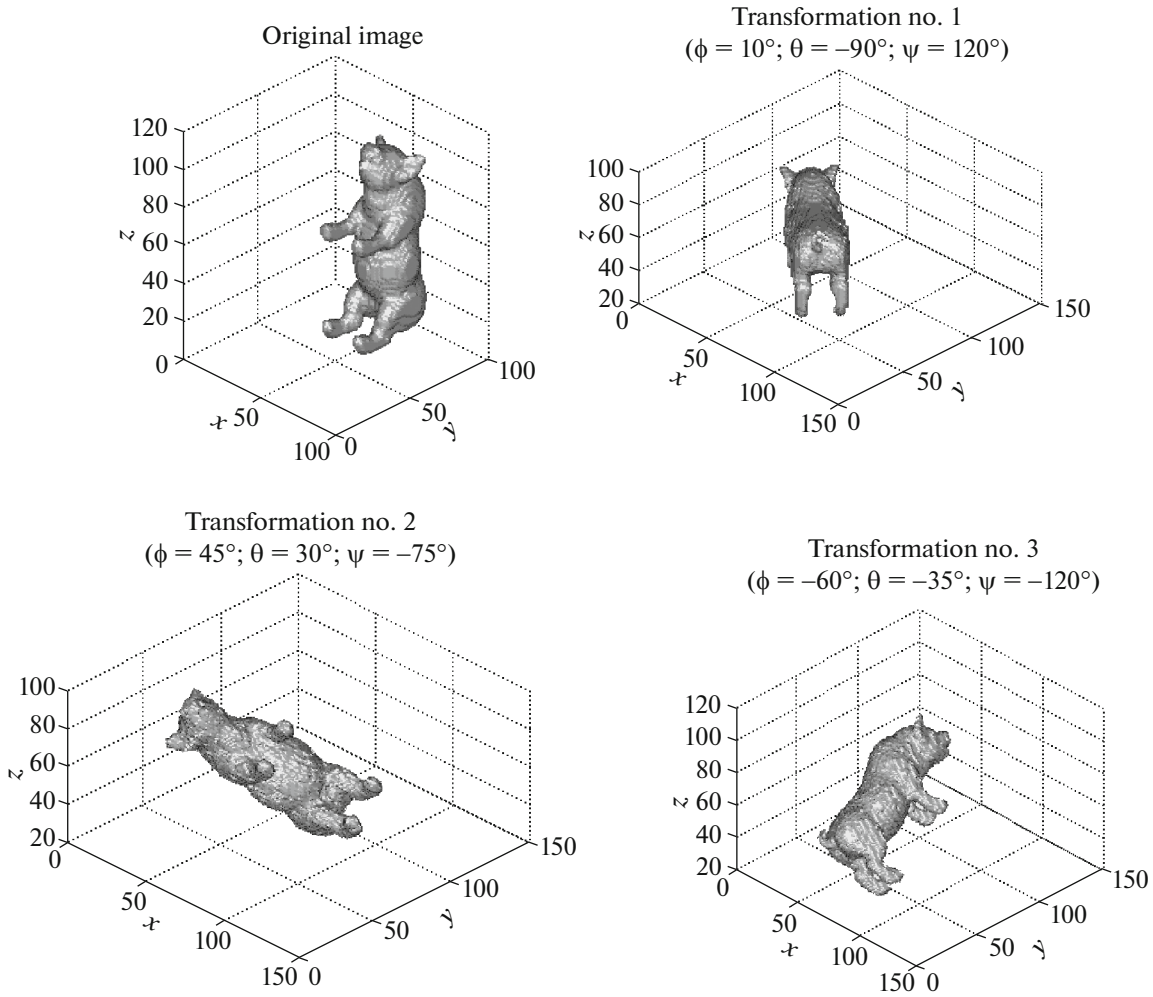

Fig. 4. A set of transformed pattern of the original teddy bear image with combination of rotation.

Table 2. The proposed extracted invariants for the teddy bear image and its transformed versions

	Original image	Transformation no. 1	Transformation no. 2	Transformation no. 3	σ/μ
Φ_{0000}	6.5520 e+13	6.5520 e+13	6.5520 e+13	6.5520 e+13	0.000000 e+00
Φ_{0001}	6.5570 e+13	6.5572 e+13	6.5571 e+13	6.5572 e+13	1.492678 e−03
Φ_{0010}	6.5541 e+13	6.5540 e+13	6.5542 e+13	6.5541 e+13	8.272308 e−03
Φ_{0100}	6.5533 e+13	6.5531 e+13	6.5532 e+13	6.5532 e+13	1.452688 e−03
Φ_{1000}	3.3279 e+13	3.3279 e+13	3.3278 e+13	3.3278 e+13	1.492612 e−03
Φ_{0011}	3.3274 e+13	3.3275 e+13	3.3276 e+13	3.3276 e+13	6.876412 e−03
Φ_{0101}	3.3280 e+13	3.3280 e+13	3.3281 e+13	3.3281 e+13	6.8764140 e−03
Φ_{1001}	2.2265 e+13	2.2266 e+13	2.2267 e+13	2.2267 e+13	6.876418 e−03
Φ_{1100}	2.2340 e+13	2.2342 e+13	2.2342 e+13	2.2341 e+13	6.876445 e−03

database of the two vectors V_{query} and V_{test}(class) using $d_{Euclidean}$ and $d_{correlation}$.

The test set also is degraded by salt and pepper noise with noise densities 1, 2, 3, and 4%. The feature vector based on 3D rotational radial Meixner's moment invariants is used to classify these images and its recognition accuracy is compared with that of 3D radial Krawtchouk moment invariants. The results of the classification using all features are presented in Table 6.

4. CONCLUSION

In this article, we propose a new set of 2D and 3D rotation invariants based on orthogonal radial Meixner moments. We have found a theoretical mathematics to derive them. Therefore, this paper introduces, in a first case, a new 2D radial Meixner moments using polar representation of an image by a one-dimensional orthogonal discrete Meixner polynomials and a circular function. In the second case, we present a new 3D radial Meixner moments using a spherical representation of volumetric image by a one-dimensional orthogonal discrete Meixner polynomials and a spherical function. Further 2D and 3D rotational invariants are derived from the proposed 2D and 3D radial Meixner moments respectively.

In order to prove the proposed approach, three issues are resolved mainly image reconstruction, rotational invariance and pattern recognition. Experimental results prove that the radial Meixner moments have perform better than the radial Krawtchouk moments in terms of volumetric image reconstruction capability simultaneously, the reconstructed volumetric image converges quickly to the original image using 2D and 3D radial Meixner moments and the test images are correctly recognized from a set of images that are available in a PSB database.

APPENDIX

Meixner moments. Meixner moments H_{nm} of order (n, m) for an intensity image $f(x, y)$ of size $N \times M$ are given by

$$DM_{nm} = \sum_{x=0}^{N-1}\sum_{y=0}^{M-1} \tilde{\omega}_n^{(\beta,\mu)}(x)\tilde{\omega}_m^{(\beta,\mu)}(y) f(x,y). \qquad (1A)$$

To ensure the numerical stability of weighted Meixner polynomial $\tilde{\omega}_n^{(\beta,\mu)}(x)$ is presented as

$$\tilde{\omega}_n^{(\beta,\mu)}(x) = \tilde{\omega}_n^{(\beta,\mu)}(x)\sqrt{\frac{w_n(x)}{d_n^2}}, \qquad (2A)$$

where $\tilde{\omega}_n^{(\beta,\mu)}(x)$ the nth order Meixner polynomial, which is defined by employing a hypergeometric function as [22]

$$\omega_n^{(\beta,\mu)}(x) = (\beta)_n\, {}_2F_1\left(\begin{matrix}-n,-x\\ \beta\end{matrix}\Big|1-\frac{1}{\mu}\right), \qquad (3A)$$

where $n \geq 0$ and $0 < \mu < 0$ and $\beta > 0$ and the generalized hypergeometric function ${}_2F_1(.)$ is definded as

Fig. 5. Collection of the COIL-20 objects [20].

Table 3. Classification results of COILL-20 object database by using d_1 distance

Invariant moments	Noise free, %	Salt and pepper noise, %			
		1	2	3	4
Radial Krawtchouk	100	89.62	86.15	80.47	61.16
Proposed method	100	93.12	90.22	85.25	62.43

Table 4. Classification results of COILL-20 object database by using d_2 distance

Invariant moments	Noise free, %	Salt and pepper noise, %			
		1	2	3	4
Radial Krawtchouk	100	89.61	86.25	80.97	61.36
Proposed method	100	93.12	90.762	84.35	62.03

$$ {}_2F_1\left(\begin{matrix}a_1,a_2\\ b_1\end{matrix}|z\right)=\sum_{i=0}^{\infty}\frac{(a_1)_i(a_2)_i}{(b_1)_i}\frac{z^i}{i!}, \tag{4A}$$

and the Pochhammer symbol $(\alpha)_i$ is given by

$$(\alpha)_i=\alpha(\alpha+1)\ldots(\alpha+i-1)=\frac{\Gamma(\alpha+i)}{\Gamma(\alpha)} \tag{5A}$$

$$\text{with}\quad \Gamma(x+1)=x!, \tag{6A}$$

and $w_n(x)$ the weight function

$$w_n(x)=\frac{\mu^{x+n}\Gamma(n+\beta+x)}{\Gamma(\beta)\Gamma(x+1)}, \tag{7A}$$

and the square norm d_n^2 is defined as

$$d_n^2=\frac{\Gamma(n+1)(\beta)_n}{\mu^n(1-\mu)^\beta}. \tag{8A}$$

With the orthogonal property of normalized orthogonal polynomial can be rewritten as

$$\sum_{x=0}^{N-1}\tilde{\omega}_n^{(\beta,\mu)}(x)\tilde{\omega}_m^{(\beta,\mu)}(x)=\delta_{nm} \tag{9A}$$

with δ_{nm} denote the Dirac function.

The recurrence relation respect to n of Meixner polynomials are defined as

$$A_n\tilde{\omega}_n^{(\beta,\mu)}(x)=B_nD_n\tilde{\omega}_{n-1}^{(\beta,\mu)}(x)+C_nE_n\tilde{\omega}_{n-2}^{(\beta,\mu)}(x), \tag{10A}$$

where

$$A_n=\frac{\mu}{\mu-1},$$

$$B_n=\frac{x-x\mu+\mu-n+1-\beta\mu-\mu n}{1-\mu},$$

$$C_n=-\frac{(n-2+\beta)(n-1)}{1-\mu},$$

$$D_n=\sqrt{\frac{\mu}{n(\beta+n-1)}},$$

$$E_n=\sqrt{\frac{\mu^2}{n(n-1)(\beta+n-2)(\beta+n-1)}}$$

with $n\geq 2$.

The first orders of discrete normalized Meixner polynomials are calculated from the above equations

$$\tilde{\omega}_0^{(\beta,\mu)}(x)=\sqrt{\frac{w_0(x)}{d_0^2}}=\sqrt{\frac{(1-\mu)^\beta(\beta+x-1)!\mu^x}{(\beta-1)!x!}}, \tag{11A}$$

$$\begin{aligned}\tilde{\omega}_1^{(\beta,\mu)}(x)&=\left(x-\frac{x}{\mu}+\beta\right)\sqrt{\frac{w_1(x)}{d_1^2}}x\\ &=\left(x-\frac{x}{\mu}+\beta\right)\sqrt{\frac{\mu(1-\mu)^\beta\mu^x(x+\beta-1)!}{(\beta-1)!x!}}.\end{aligned} \tag{12A}$$

The weighted Meixner polynomials form an orthonormal system, the reconstruct image can be deduced by

$$f(x,y)=\sum_{n=0}^{N-1}\sum_{m=0}^{M-1}\tilde{\omega}_n^{(\beta,\mu)}(x)\tilde{\omega}_m^{(\beta,\mu)}(y)DM_{nm}. \tag{13A}$$

For computed the 2D moments to order $M_{\max}$, we can approximated the reconstructed image in Eq. (13A) by

$$f_{\text{rec}}(x,y)=\sum_{x=0}^{\max-1}\sum_{y=0}^{\max-1}\tilde{\omega}_n^{(\beta,\mu)}(x)\tilde{\omega}_m^{(\beta,\mu)}(y)(x,N)DM_{nm} \tag{14A}$$

The 3D Meixner moments of order $n+m+l$ for a volumetric image function $f(x,y,z)$ of size $N\times M\times L$ are defined as

$$\begin{aligned}DM_{nml}=&\sum_{x=0}^{N-1}\sum_{y=0}^{M-1}\sum_{z=0}^{L-1}\tilde{\omega}_n^{(\beta,\mu)}(x)\tilde{\omega}_m^{(\beta,\mu)}(y)\\ &\times\tilde{\omega}_l^{(\beta,\mu)}(z)f(x,y,z).\end{aligned} \tag{15A}$$

Using the orthogonality property, The inverse transform of Meixner moments are given by

$$\begin{aligned}f(x,y,z)=&\sum_{n=0}^{N-1}\sum_{m=0}^{M-1}\sum_{l=0}^{L-1}\tilde{\omega}_n^{(\beta,\mu)}(x)\\ &\times\tilde{\omega}_m^{(\beta,\mu)}(y)\tilde{\omega}_l^{(\beta,\mu)}(y)DM_{nml}.\end{aligned} \tag{16A}$$

Table 5. The Euclidean distance and correlation coefficient between request free-noise image and same images of classes from PSB database

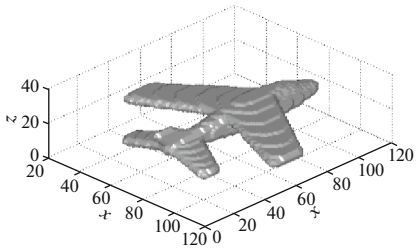

Original volumetric airplane image of size 128 × 128 × 128 voxels

	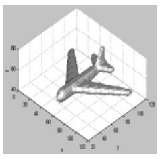	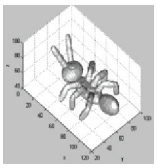	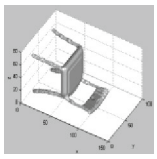	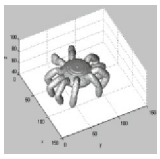	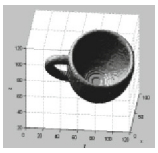
$d_{\text{Euclidien}}$	0.014	3.3287	2.8736	2.8260	2.4631
$d_{\text{correlation}}$	0.9992	0.2392	0.4541	0.3742	0.1246
	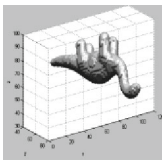	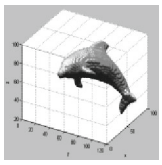	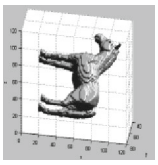	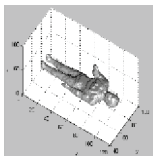	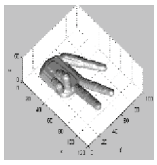
$d_{\text{Euclidien}}$	3.7735	1.7735	2.5620	4.0931	2.7377
$d_{\text{correlation}}$	0.8658	0.8991	0.2390	0.7634	0.3742
	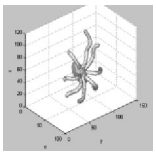	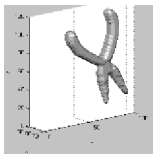	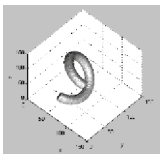	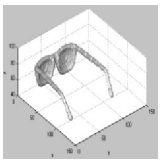	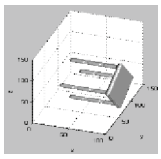
$d_{\text{Euclidien}}$	2.7416	2.8865	2.2697	3.9879	2.6452
$d_{\text{correlation}}$	0.1659	0.1235	0.1291	0.4291	0.4310

For computed the 2D moments to order $M_{\max}$, we can approximated the reconstructed image in Eq. (16A) by

$$f_{\text{rec}}(x,y,z) = \sum_{n=0}^{\max-1}\sum_{m=0}^{\max-1}\sum_{l=0}^{\max-1} \tilde{\omega}_n^{(\beta,\mu)}(x) \times \tilde{\omega}_m^{(\beta,\mu)}(y)\tilde{\omega}_l^{(\beta,\mu)}(z)DM_{nml}. \quad (17A)$$

Table 6. Classification results of Princeton shape benchmark (PSB) using $d_{\text{Euclidien}}$ distance

3D Invariant moments	Noise free, %	Salt and pepper noise, %			
		1	2	3	4
3D Radial Krawtchouk	100	89.61	86.25	80.97	61.36
Proposed method	100	93.25	90.32	85.35	69.03

REFERENCES

1. J. Flusser, T. Suk, and B. Zitová, *Moments and Moment Invariants in Pattern Recognition* (Wiley, Chichester, 2009).
2. M. El Mallahi, A. Mesbah, H. El Fadili, K. Zenkouar, and H. Qjidaa, "Compact computation of Tchebichef moments for 3D object representation," WSEAS Trans. Circuits Syst. **13**, 368–380 (2014).
3. M. El Mallahi, A. Mesbah, H. Qjidaa, K. Zenkouar, and H. El Fadili, "Translation and scale invariants of three-dimensional Tchebichef moments," *in Proc. 2015 Intelligent Systems and Computer Vision* (*ISCV*) (IEEE, 2015), pp. 1–5.
4. M. El Mallahi, A. Mesbah, H. Qjidaa, A. Berrahou, K. Zenkouar, and H. El Fadili, "Volumetric image reconstruction by 3D Hahn moments," in Proc. 2015 IEEE/ACS 12th Int. Conf. on Computer Systems and Applications (AICCSA) (IEEE, 2015), pp. 1–8.
5. M. El Mallahi, A. Zouhri, A. Mesbah, and H. Qjidaa, "3D radial invariant of dual Hahn moments," Neural Comput. Applic., pp. 1–12 (2016). doi: 10.1007/s00521-016-2782-x

6. A. Mesbah, M. El Mallahi, H. El Fadili, K. Zenkouar, A. Berrahou, and H. Qjidaa, "An algorithm for fast computation of 3D Krawtchouk moments for volumetric image reconstruction," in *Proceedings of the Mediterranean Conference on Information Communication Technologies 2015, MedCT 2015*, Vol. 1, Ed. by A. El Oualkadi, F. Choubani, and A. El Moussati, Lecture Notes in Electrical Engineering (Springer, Cham, 2016), Vol. 380, pp. 267–276.
7. A. Mesbah, A. Berrahou, M. El Mallahi, and H. Qjidaa, "Fast algorithm for 3D local feature extraction using Hahn and Charlier moments," in *Advances in Ubiquitous Networking 2, Proc. of the Unet'16*, Ed. by R. El-Azouzi et al., Lecture Notes in Electrical Engineering (Springer, Singapore, 2016), Vol. 397, pp. 375–373.
8. A. Mesbah, A. Berrahou, M. El Mallahi, and H. Qjidaa, "Fast and efficient computation of three-dimensional Hahn moments," J. Electron. Imaging **25** (6), 061621, 12 pages (2016).
9. A. Mesbah, A. Zouhri, M. El Mallahi, K. Zenkouar, and H. Qjidaa, "Robust reconstruction and generalized dual Hahn moments invariants extraction for 3D images," 3D Research **8** (1), Article 7, 20 pages (2017).
10. J. Flusser, T. Suk, and B. Zitová, *Moments and Moment Invariants in Pattern Recognition* (Wiley, Chichester, 2009).
11. M. El Mallahi, A. Zouhri, J EL-Mekkaoui, and H. Qjidaa, "Three dimensional radial Tchebichef moment invariants for volumetric image recognition," Pattern Recogn. Image Anal. **27** (4), 810–824 (2017).
12. B. Xiao, Y. Zhang, L. Li, W. Li, and G. Wang, "Explicit Krawtchouk moment invariants for invariant image recognition," J. Electron. Imaging **25** (2), 023002, 10 pages (2016).
13. M. El Mallahi, A. Zouhri, A. Mesbah, A. Berrahou, I. El Affar, and H. Qjidaa, "Radial invariant of 2D and 3D Racah moments," Multimed. Tools Appl. **77** (6), 6583–6604 (2017).
14. H. S. Hsu and W. H. Tsai, "Moment-preserving edge detection and its application to image data compression," Opt. Eng. **32** (7), 1596–1608 (1993).
15. X.-Y. Wang, P.-P. Niu, H.-Y. Yang, et al., "A new robust color image watermarking using local quaternion exponent moments," Inform. Sci. **277**, 731–754 (2014).
16. M. El Mallahi, A. Zouhri, A. El Affar, A. Tahiri, and H. Qjidaa, "Radial Hahn moment invariants for 2D and 3D image recognition," Int. J. Autom. Comput., 1–13 (2017). doi: 10.1007/s11633-017-1071-1
17. M. Kazhdan, "An approximate and efficient method for optimal rotation alignment of 3D models," IEEE Trans. Pattern Anal. Mach. Intell. **29** (7), 1221–1229 (2007).
18. J. Fehr, "Local rotation invariant patch descriptors for 3D vector fields," in *Proc. 2010 20th Int. Conf. on Pattern Recognition* (*ICPR'10*) (IEEE Computer Society, 2010), pp. 1381–1384.
19. J. Fehr and H. Burkhardt, "3D rotation invariant local binary patterns," in *Proc. 2008 19th Int. Conf. on Pattern Recognition* (*ICPR'08*) (IEEE Computer Society, 2008), pp. 1–4.
20. H. Skibbe, M. Reisert, and H. Burkhardt, "SHOG–Spherical HOG descriptors for rotation invariant 3D object detection," in *Pattern Recognition, DAGM 2011*, Ed. by R. Mester and M. Felsberg, Lecture Notes in Computer Science (Springer, Berlin, 2011), Vol. 6835, pp. 142–151.
21. N. Canterakis, "3D Zernike moments and Zernike affine invariants for 3D image analysis and recognition," in *Proc. 11th Scandinavian Conf. on Image Analysis SCIA'99, Greenland, 1999*, Ed. by B. K. Ersbøll and P. Johansen (DSAGM, 1999), Vol. 1, pp. 85–93.
22. H. Zhu, H. Shu, J. Zhou, L. Luo, and J. L. Coatrieux, "Image Analysis by discrete orthogonal dual Hahn moments," Pattern Recogn. Lett. **28** (13), 1688–1704 (2007).
23. http://www.cs.columbia.edu/CAVE/software/softlib/coil-20.php
24. Princeton, Princeton Shape Benchmark, 2013. http://shape.cs.princeton.edu/benchmark/

Mostafa El Mallhi received the B.Sc, M.Sc, and Ph. D. degrees in computer science from Faculty of Sciences, University Sidi Mohammed Ben Abdellah, Morocco in 2000, 2007, and 2017, respectively. His research interests include image processing, pattern classification, orthogonal systems, neural networks, big data, data mining, data science, deep learning, genetic algorithms, and special functions.

Amal Zouhri received the B.Sc, M.Sc, and Ph.D. degrees in electrical engineering from Faculty of Sciences, Sidi Mohammed Ben Abdellah University, Morocco in 2008, 2011, and 2016, respectively. Her research interests include embedded system, stability and stabilization of interconnected systems, decentralized systems, robust and H∞ control, linear matrix inequalities LMIs, singular systems, time delay systems, computer science.

Professor Hassan Qjidaa received his M.Sc and PhD in applied physics from Claud Bernard University of Lyon France in 1983 and 1987, respectively. He got the Pr. Degree in Electrical Engineering from sidi mohammed Ben Abdellah university, Fez, Morocco 1999. He is now an professor in the Dept. of physics in Sidi Mohammed Ben Aabdellah university, Fez, Morocco. His main research interest include image manuscripts recognition, cognitive science, image processing, computer graphics, pattern recognition, neural networks, human-machine interface, artificial intelligence and robotics.